Journal of ELECTRONIC MATERIALS, Vol. 44, No. 4, 2015
DOI: 10.1007/s11664-015-3636-5

A Comparative Study of Nanostructured TiO_2, ZnO and Bilayer TiO_2/ZnO Dye-Sensitized Solar Cells

MAMTA RANI[1,2] and S.K. TRIPATHI[1,3,4]

1.—Department of Physics, Centre of Advanced Study in Physics, Panjab University, Chandigarh, Chandigarh 160014, India. 2.—Department of Physics, DAV University, Jalandhar, Punjab 144012, India. 3.—e-mail: surya@pu.ac.in. 4.—e-mail:surya_tr@yahoo.com

Titanium dioxide (TiO_2), Zinc oxide (ZnO) and bilayer TiO_2/ZnO (TZO) based cells have been developed and sensitized with five organic dyes and one cocktail dye composed of five dyes. Photovoltaic performance of TiO_2 and ZnO solar cell sensitized with six dyes is compared to that of bilayer TZO cells. The forward current is found to increase with applied voltage in the range $V \leq 0.4$ V, which is dominated by thermionic emission, whereas in $0.4 \leq V \leq 0.7$ V, the current transport is due to space charge-limited current controlled by exponential trap distribution in all devices. The combined properties of the materials enhance the efficiency of composite TZO cells. TiO_2 permits the formation of an energy barrier at the ZnO electrode/electrolyte interface, which reduces the back electron transfer from the conduction band of ZnO to I_3^- in the electrolyte. Also, due to the TiO_2 layer on the ZnO, the latter forms a compact layer between flourine-doped tin oxide (FTO)/TiO_2 which benefits the fast electron transfer from TiO_2 to ZnO to FTO glass. This reduces the charge recombination occurring at the ZnO/FTO interface leading to higher open circuit voltage (V_{oc}), higher short circuit current (J_{sc}), lower series resistance (R_s), and in turn higher efficiency in TZO solar cells as compared to ZnO cells. Among the six dyes, Eosin-Y and Rose Bengal dye gave the best performance as sensitizers with TZO.

Key words: TZO, dye-sensitized solar cell, conversion efficiency, organic dye

INTRODUCTION

Dye-sensitized solar cells (DSSCs) have attracted great attention as a promising photovoltaic technologies alternative to thin films solar cells, owing to their low cost production, usage of medium purity materials and impressive incident photons to electrical current conversion efficiency and long-term stability.[1,2] A typical DSSC is an electrochemical device, which is composed of a nanocrystalline semiconductor film, sensitizing dye, electrolyte, and counter electrode. The dye is promoted into an excited state upon light absorption from where an ultrafast electron injection process takes place into the conduction band of the semiconductor. The presence of the redox couple in the electrolyte and suitable energy band positioning ensure the regeneration of the dye as well as diffusion of the charge. The oxide material plays a fundamental role in device functioning. It acts as a substrate for the dye, controls the energy alignment of the excited state of the dye, which eventually controls the charge transfer, and it is the main source of electron recombination. Binary metal oxides such as TiO_2, ZnO, Nb_2O_5, Fe_2O_3, ZrO_2, Al_2O_3, CeO_2 and ternary compounds such as $SrTiO_3$, Zn_2SnO_4 have been tested for their use as photoelectrodes in DSSC.[3] Among them, the d-block binary metal oxides, TiO_2, ZnO, and Nb_2O_5 are the best candidates to be photoelectrodes due to the dissimilarity in orbitals constituting their conduction band and valence band.[3]

The high efficiency of these DSSCs depends upon the effective separation and transportation of the charges generated in the dye molecules over the

(Received May 27, 2014; accepted January 8, 2015; published online February 7, 2015)

semiconducting nanoparticles. However, the energy conversion efficiency of DSSCs is still inferior to conventional Si and thin films solar cells. This is a hindrance to their commercialization. In this context, the development of a new sensitizer has played a decisive role in enhancing overall efficiency and device stability, but the theoretical limit of 26.8%[4] for DSSC remains far from reach. An additional factor that influences the efficiency of a DSSC is the open circuit voltage (V_{oc}). To enhance efficiency, some researchers have attempted to improve the properties of the TiO_2 electrode[5–7] or used a bilayer system.[8,9] This bilayer electrode is obtained by coating another metal oxide on a base metal oxide electrode. This reduces the recombination rate of photo-injected electrons by efficient spatial separation of photo-injected electrons, while some authors have reported improvements by appropriate modifications of the electrolyte or dye.[10–12]

As a result of a considerable review of experimental data, it has been suggested that the electron transport in nanocrystalline TiO_2 films may be the factor that limits the overall efficiency of TiO_2 based solar cells in spite of the high porosity of TiO_2.[13,14] Many attempts have been made to improve the original DSSC design and circumvent its inherent limitations, especially the low conductivity of the TiO_2 nanoparticle film and potential charge recombination at the TiO_2 surface.[15] ZnO is an attractive material and has been widely investigated for its optical, catalytic, conductivity, and photoelectrochemical properties and for applications in piezoelectric devices,[16] ultraviolet (UV) light-emitting diodes,[17] in UV sensors[18] and in solar cells.[19] The electron mobility is much higher in ZnO than in TiO_2.[20] To get the benefits of both constituent properties, i.e. high porosity of TiO_2 and high electrical conductivity of ZnO, bilayer film has been prepared. Apart from this, the CB edge of both oxides at the same level[21] acts as an added advantage in a bilayer structure. In our report on the fabrication, characterization and photoconducting behavior of a ZnO, TiO_2 and TZO bilayer system, it has been demonstrated that the TZO is highly photoconducting and photosensitive at room temperature, which can lead to high J_{sc} in solar devices.[22] The composite ZnO/TiO_2 films have been developed with the aim of producing solar cells with improved photovoltaic properties compared to those displayed by either ZnO or TiO_2 cells. All cells presented here have been sensitized with the six low-cost organic dyes, which are commonly used with TiO_2[23,24] and ZnO.[25–27]

EXPERIMENTAL DETAILS

ZnO, TiO_2 and bilayer TZO films were prepared as by using the doctor blade method. For this, the colloidal solution is made by dissolving 16 mL of titanium butoxide ($Ti(OC_4H_9)_4$) in 8 mL ethyl alcohol (EtOH). The solution was added dropwise to a solution of H_2O and concentrated H_2SO_4. The mole ratio of $Ti(OC_4H_9)_4$:H_2O:C_2H_5OH was about 1.3: 320.6:3.9. The above solution was aged at 353 K for 30 min. A clear solution was obtained after 7 days. The filtered residue was dried at 353 K for 6 h and then ground to a fine powder to get a dried gel. The dried gel was calcined in air for 6 h at 873 K to obtain nanosized TiO_2 powder. Selection of temperature range from 873 K is based on all organic residue burning up at 673 K, while above 873 K, anatase starts to convert into rutile phase, having less porosity, as reported in literature. The high porosity is a crucial factor for adsorption of dye. In our previous study,[28] the x-ray diffraction (XRD) and transmission electron microscopy (TEM) of TiO_2 at 673 K, 773 K and 873 K was mentioned. The XRD pattern of TiO_2 nanoparticles annealed at those temperatures confirmed the anatase phase of TiO_2. Transformation was confirmed by the appearance of a detectable rutile peak by XRD at 873 K. The TEM image of anatase phase of TiO_2 obtained at 673 K consisted of well-dispersed nanorods with an aspect ratio of about 7:1. The TEM image of TiO_2 nanorods calcined at 773 K revealed the gradual increase in both diameter and length.[28] Further increasing the calcination temperature to 873 K, small nanorods agglomerated to form large nanorods, which showed more porous irregular networks as is clear from the TEM image at 100 nm scale at 873 K. Also, for ZnO at 673 K to 873 K, we obtained the wurtzite phase. TEM and XRD of ZnO at 673 K are reported in Ref. 29. So, the selected calcination temperature was 873 K for the application of TiO_2, ZnO and TZO films in DSSC.

A 0.1 M ZnO solution was prepared by dissolving zinc acetate dehydrate in methanol at room temperature. The pH value of the solution was adjusted to 10.5 using sodium hydroxide (1 M) solution. The resulting filtrate was kept for 48 h to complete the gelation and hydrolysis process. The ZnO gel was first dried at 373 K for 2 h and then annealed in air at 723 K for 30 min. PEG (polyethylene glycol) was added to the TiO_2 and ZnO nanopowder separately to prevent the aggregation of the particles and to improve the porosity of the films. TZO film was prepared by coating TiO_2 nanorods on prepared ZnO film and sintering at 723 K. The thickness of the sintered TiO_2, ZnO films was 5 μm and that of TZO film was 10 μm. Six organic dyes, Eosin Y (EY), Fast Green (FGF), Rose Bengal (Rose), Rhodamine B (RhB), Acridine orange (AO), and Cocktail dye (C) were used for sensitizing the metal oxide films. The dyes were dissolved in ethanol having a concentration of 3.0×10^{-4} M. Cocktail dye solution was prepared by mixing different dyes at specific concentrations as reported by Seema et al.[30] Dye-sensitized photoelectrodes were prepared by dipping the film in the different dye solutions for 48 h. The films were then rinsed with ethanol. A sandwich-type DSSC was fabricated with the dye-sensitized oxide electrode and platinum-coated FTO as counter electrode and electrolyte. The counter electrode was

prepared by thermal decomposition of hexachloroplatinic acid solution in isopropanol on FTO. The electrolyte solution was a mixture of 0.5 M KI and 0.05 M iodine in an ethylene carbonate and acetonotrile mixed solvent (60:40 by volume).

UV–Visible absorption spectra of all the dye-sensitized metal oxide photoelectrodes were recorded on a Perkin Elmer LS-35 spectrometer. Solar cell performance was studied in the standard solar cell laboratory of the Solar Energy Centre (SEC), Ministry of New and Renewable Energy, Gurgaon, using a class AAA solar simulator model SP1000-4966-based Solar Cell Tester of M.S Oriel, USA, to study under standard test conditions (STC). Photoelectrochemical data were measured using a 1600-W Xenon light source that was focused to give 1000 Wm^{-2} equivalent to 1 sun at AM 1.5 at the surface of the test cell. The working distance of the lamp was 12.00 ± 0.5 cm. Current–voltage (I–V) characteristics of the cell were recorded using a four-point probe Keithley source meter (Model 2400). The active area was typically 1 cm^2.

RESULTS AND DISCUSSION

Fourier transform infrared (FTIR) results confirm the formation of TZO film.[22] Direct band gap energy for ZnO, TiO_2 and TZO film was 3.2 eV, 3.59 eV and 3.0 eV, respectively, as reported earlier.[22,28,29] TZO had broader absorption as compared to ZnO. ZnO and TZO nanopowder films were sensitized with the five types of commercially available organic dyes, EY, FGF, Rose, RhB, and AO, and the C dye composed of these five dyes. The absorption spectra of these dyes in solution and adsorbed on the ZnO and TZO films are displayed in Figs. 1 and 2. In solution, the absorption peaks are observed at 529 nm for EY, 617 nm for FGF, 558 nm for Rose, 544 nm for RhB, and 490 nm for AO. The Cocktail dye has three absorption maxima at 495 nm, 539 nm and 615 nm. When the dyes are attached to the oxide films, the absorption peaks are shifted as compared to the spectra in solution. The device sensitized with cocktail dye has a much stronger optical absorption compared with the five dyes in the broad visible region. The shifts of the absorption spectra by adsorption on the oxide surface have also been observed in other organic dyes[31] and may be attributed to a strong interaction between the anchoring group of the dye and the semiconductor surface.[2] This kind of interaction also leads to an aggregated state of the dye on the film. Although π–π stacking of organic dyes is advantageous for light harvesting because of its broad features in the UV–Vis absorption spectrum, it is important to emphasize that only the dye covalently attached to the oxide surface by the anchoring group will contribute to the change in the conductivity of the device. UV–Vis absorption spectra of all dye-sensitized oxide films demonstrate that the dyes are completely anchored with all the ZnO and TZO films and that these compounds absorb light of appropriate wavelengths which indicates that they can be used as photosensitizers for wide band gap semiconductors which on their own cannot adsorb visible light.

Figures 3, 4 and 5 represent the dark J–V characterstics on a semi-logarithmic scale of the solar cells made with metal oxide/dye/KI using TiO_2, ZnO and TZO (TiO_2/ZnO) and sensitized with six dyes, EY, FGF, Rose, RhB, AO and C. The current density–volatge (J–V) characteristics of the prepared DSSC were found to be non-linear. The deviation from linearity can be attributed to the series resistance, bulk resistance and the interface state properties of the DSSC device. Resistance is the important factor for scaling the performance of metal-oxide/dye/KI soalr cells. The existence of an interfacial layer and series resistance affects the ideality factor of the diode. From the dark characterstics of solar cells, the values of built-in voltage

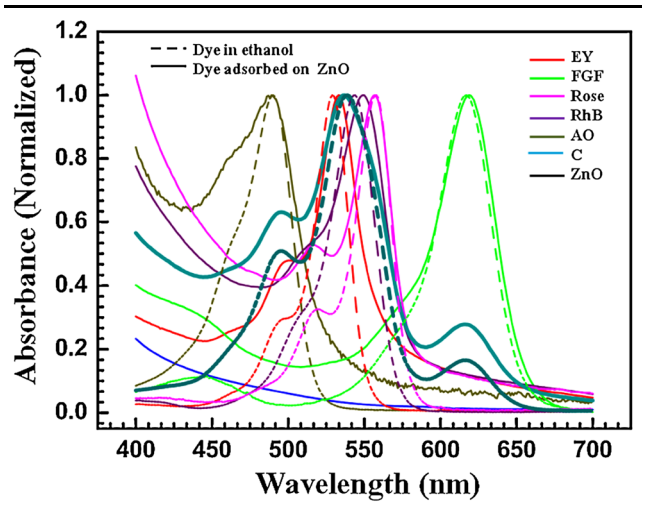

Fig. 1. Normalized UV–Vis absorbance spectra of six dyes in ethanol solution and adsorbed on a ZnO electrode.

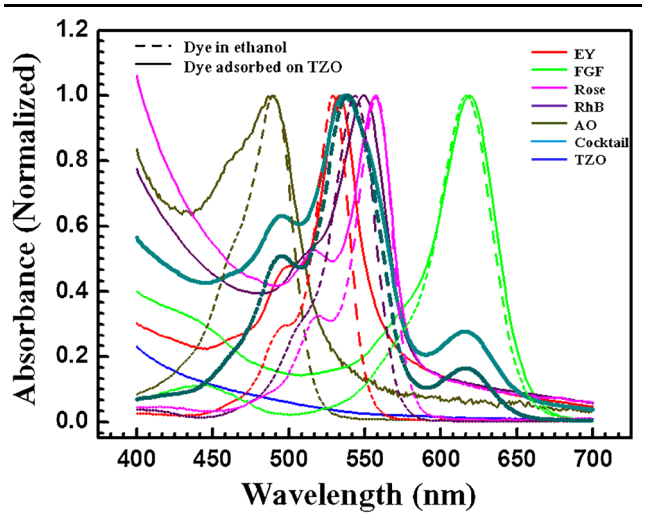

Fig. 2. Normalized UV–Vis absorbance spectra of six dyes in ethanol solution and adsorbed on a TZO electrode.

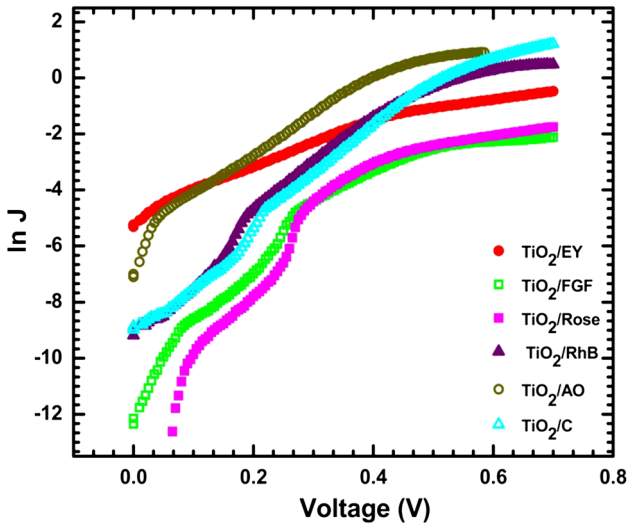

Fig. 3. Semi-logarithmic plot of the dark *I–V* characteristics of the prepared TiO_2 dye.

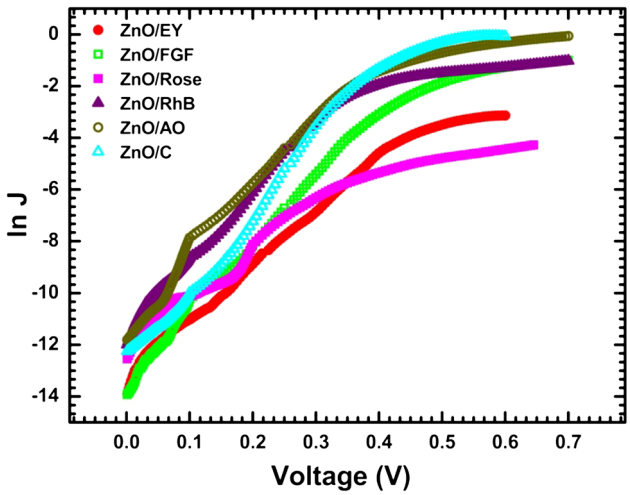

Fig. 4. Semi-logarithmic plot of the dark *I–V* characteristics of the prepared ZnO dye.

(V_{bi}), breakdown voltage (V_{Bd}) and breakdown current (I_{Bd}) were found and are listed in Table I.

Different regions of the *J–V* curve are dominated by different loss mechanisms. So, Eq. 1 is fitted with the lower part of the dark *J–V* curve in the region ($V < 0.4$ V). The plot of ln (I) versus V is a straight line. The value of slope = q/nk_BT gives the value of ideality factor and the y-intercept gives the value of I_s.[32] The values of I_s and n for all the diodes are listed in Table I.

The saturation current is given by[33]

$$I_s = AA^*T^2\exp\left[-\frac{q\phi_B}{k_BT}\right], \quad (1)$$

where $A^* = 4\pi qm^*k_B^2/h^3$ is the Richardson constant, m^* is the effective mass of the carriers, ϕ_B is the potential barrier height, T is the device temperature

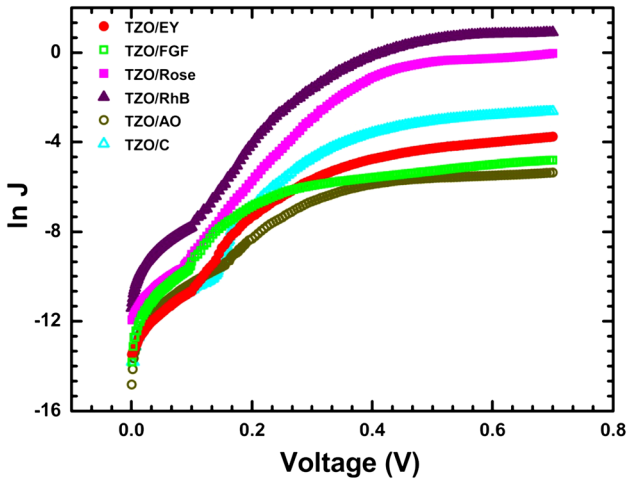

Fig. 5. Semi-logarithmic plot of the dark *I–V* characteristics of the prepared TZO dye-sensitized solar cells.

and A is the device area. There is a lot of variation in the electron effective mass value of TiO_2. Monticone et al. take the anatase TiO_2 electron effective mass $m_e^* = 10\ m_o$.[34] On the one hand, Pascual and coworkers obtained $m_e^* = 3\ m_0$,[35] whereas Stamate reported a value of $m_e^* = (0.71–1.26)\ m_o$.[36] We considered the intermediate value ($m_e^* = 3\ m_o$). Effective mass of ZnO is 0.29 m_o and TZO is 1.65 m_o. The values of the Richardson constant using the above value of effective mass for TiO_2, ZnO and TZO are 35.12, 363.33 and 199.23, respectively.

On taking the log on both side of Eq. 1, we get

$$\ln I_s = \ln AA^*T^2 - \frac{q\phi_B}{k_BT}, \quad (2)$$

which gives

$$\phi_B = \frac{k_BT}{q}\ln\frac{AA^*T^2}{I_s}. \quad (3)$$

The value of ϕ_B calculated using the above equation is tabulated in Table I. The ideality factor higher than unity represents the non-ideal behavior of J-V characteristics at lower voltages. The non-ideality decreases the photocurrent in the solar cell by diffusion of the iodide or tri-iodide ions within the nano-structured oxide film.[37] The higher value of n may be due to the potential drop in the interfacial layer and the presence of excess current, and to the recombination current through the interfacial states between the metal insulator layers. There are different possible factors which can affect the ideality values such as: series resistance, image forces, tunnelling, generation-recombination, interface impurities and interfacial oxide layer.[38,39]

The double logarithmic plots of forward *J–V* charateristics in voltage range ($0.4 < V \le 0.7$) are shown for TiO_2, ZnO and TZO in Figs. 6, 7, and 8, respectively.

Table I. Current–voltage (*J–V*) parameters: ideality factor (n), potential barrier height (ϕ_B), reverse saturation current (I_s), built-in voltage (V_{bi}), breakdown volatge (V_{Bd}), SPLC exponent (m), and characteristic temperature (T_t)

Samples	n	ϕ_B (eV)	I_s (A)	V_{bi} (V)	V_{Bd} (V)	m	T_t (K)
TiO_2/EY	4.42	0.58	7.37×10^{-3}	0.22	−0.43	2.52	1518
TiO_2/FGF	1.85	0.73	1.73×10^{-5}	0.32	−0.32	4.43	1029
TiO_2/Rose	1.49	0.77	3.06×10^{-6}	0.28	−0.63	6.06	454
TiO_2/RhB	1.84	0.69	8.87×10^{-5}	0.37	−0.40	5.10	1231
TiO_2/AO	2.60	0.60	3.27×10^{-3}	0.30	−0.30	4.16	949
TiO_2/C	1.98	0.69	8.96×10^{-5}	0.42	−0.50	5.72	1415
ZnO/EY	1.78	0.79	1.90×10^{-6}	0.35	−0.53	6.57	1671
ZnO/FGF	1.26	0.81	1.05×10^{-6}	0.36	−0.60	7.38	1914
ZnO/Rose	2.33	0.75	9.15×10^{-6}	0.26	−0.63	3.21	663
ZnO/RhB	1.39	0.75	1.05×10^{-5}	0.24	−0.61	6.03	1509
ZnO/AO	1.26	0.76	7.25×10^{-6}	0.30	−0.61	5.89	1467
ZnO/C	1.10	0.80	1.97×10^{-6}	0.34	−0.65	8.08	2124
TZO/EY	1.66	0.76	2.88×10^{-6}	0.24	−0.58	3.28	685
TZO/FGF	2.03	0.73	9.38×10^{-6}	0.20	−0.55	1.45	136
TZO/Rose	1.35	0.74	8.08×10^{-6}	0.30	−0.66	6.15	1545
TZO/RhB	1.36	0.73	1.33×10^{-5}	0.29	−0.58	4.98	1196
TZO/AO	2.03	0.75	4.18×10^{-6}	0.20	−0.64	2.79	539
TZO/C	1.46	0.77	2.44×10^{-6}	0.25	−0.59	4.07	921

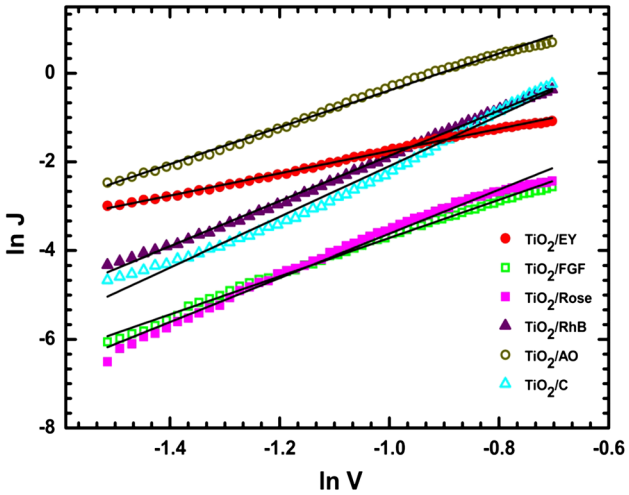

Fig. 6. Double-logarithmic plot of the dark forward *I–V* characteristics of the prepared TiO_2 dye-sensitized solar cells.

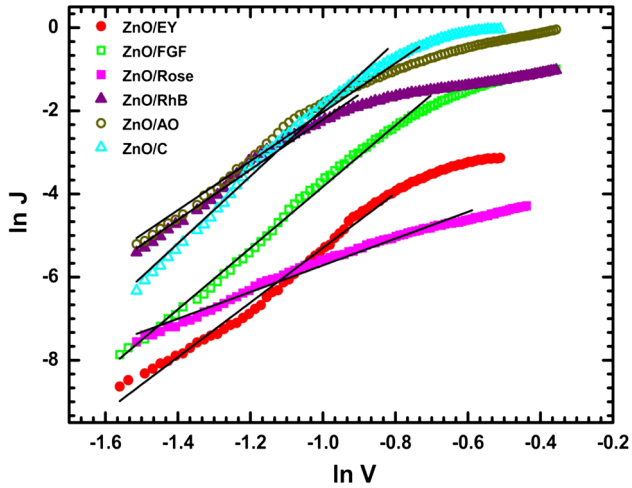

Fig. 7. Double-logarithmic plot of the dark forward *I–V* characteristics of the prepared ZnO dye-sensitized solar cells.

The results exhibit a linear relationship up to a certain voltage range and the current follows the voltage dependence $I \propto V^m$. $m \sim 1$ corresponds to the Ohmic conduction, while the $m \geq 1$ case is interpreted as an indication of the space charge-limited conduction mechanism (SCLC). The value of exponent m for each sample is reported in Table I. The value of m is greater than 2 for all devices except for the TZO/FGF-based solar cell. This means that the current in the device is controlled by the SCLC mechanism dominated by exponential trap distribution. The semiconductors may contain a large number of localized defect states in their forbidden gap. Semiconductor localized states act as carrier trapping centers. Carriers from electrodes trapped in these centers and these localized states become charged. Subsequently, a space charge region would be built up in the material, which has a strong effect on the *J–V* characteristics of a device, especially at higher bias levels. So, at high voltage, the trapped carriers contribute to the conduction paths and reliable information about the density of states can be deduced from the *J–V* characteristics. In this model, the relationship between voltage and current is expressed as.[40,41]

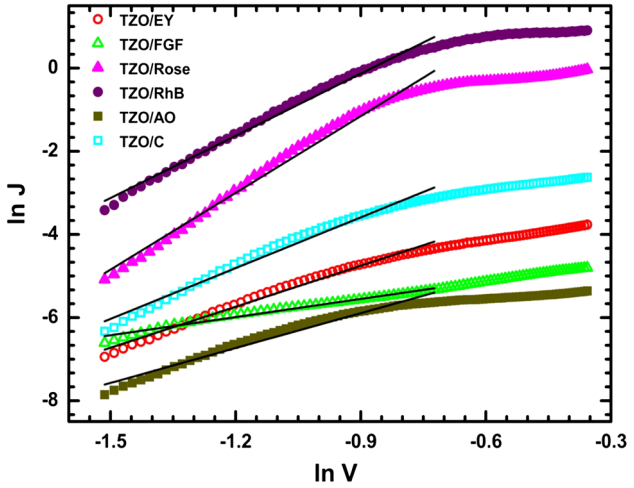

Fig. 8. Double-logarithmic plot of the dark forward *I–V* characteristics of the prepared TZO dye-sensitized solar cell.

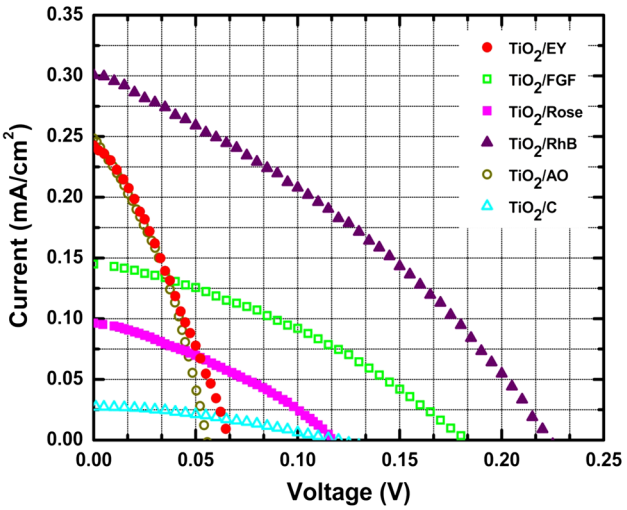

Fig. 9. Light *I–V* curve of the TiO_2 dye-sensitized solar cells.

$$I = \frac{e\mu N}{d^{2l+1}} \left(\frac{\in \in_o}{eP_o k_B T_t} \right)^l V^{l+1}, \tag{4}$$

where ε is the dielectric constant of the effective layer, e is the electronic charge, μ is the mobility of carrier charges, N is the effective density of states in electronic band edge, d is the thickness, and l is the ratio T_t/T where T_i and T_t represents the room and characteristic temperature of the exponential trap distribution, respectively. T_t is given by

$$P(E) = P_o \exp\left(\frac{-E}{k_B T_t}\right), \tag{5}$$

where $P(E)$ is the concentration of traps per unit energy range above the valence band edge. The total concentration of traps N_t is given as follows:

$$N_t = P_o k_B T_t \tag{6}$$

The value of parameters N_t, T_t, l and P_o can be found by studying the variation of LnI versus $1/T$ at different voltages.

The *J–V* curves for all dye-sensitized TiO_2, ZnO solar cells and dye-sensitized TZO under illumination are shown in Figs. 9, 10 and 11, respectively. The figures of merit (V_{oc}, J_{sc}, FF, J_{max}, P_{max}, η, R_s, R_{sh}) for these solar cells are listed in Table II. Several conclusions can be drawn from these *J–V* characteristics. The addition of TiO_2 to ZnO layer increases the V_{oc} and J_{sc} as compared to pure TiO_2- and ZnO-based solar cells with all organic dyes except the cocktail dye.

Figure 12 shows different processes involved in charge injection from metal oxide into liquid electrolyte in DSSCs. Electrons can be injected from excited dye molecules to the conduction band of ZnO and from the FTO to trap states of ZnO. For solar cell applications, the injection of these electrons into

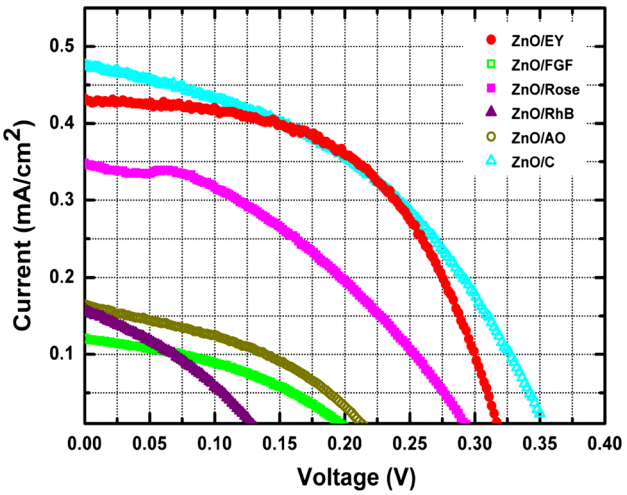

Fig. 10. Light *I–V* curve of the ZnO dye-ensitized solar cells.

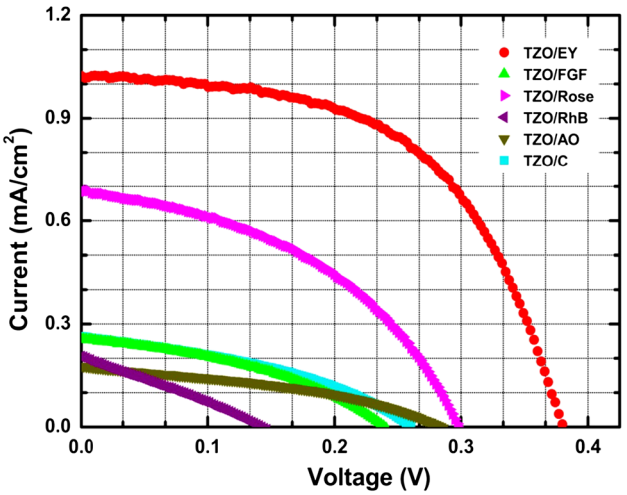

Fig. 11. Light *I–V* curve of the TZO dye-sensitized solar cells.

Table II. The figures of merit for all prepared DSSCs

Sample	V_{oc} (Mv)	J_{sc} (mA/cm^2)	J_{max} (mA/cm^2)	P_{max} (mW/cm^2)	F.F (%)	η (%)	R_s (Ω)	R_{sh} (Ω)
TiO_2/EY	66	0.241	0.150	0.005	31	0.005	665	1845
TiO_2/FGF	182	0.145	0.099	0.010	38	0.010	325	2178
TiO_2/Rose	116	0.096	0.056	0.004	36	0.004	552	1650
TiO_2/RhB	223	0.301	0.272	0.036	53	0.036	250	2560
TiO_2/AO	55	0.248	0.150	0.005	37	0.005	455	1877
TiO_2/C	121	0.028	0.026	0.002	30	0.002	670	1478
ZnO/EY	319	0.431	0.337	0.074	54	0.08	178	8862
ZnO/FGF	203	0.120	0.076	0.010	39	0.01	731	4388
ZnO/Rose	296	0.343	0.237	0.041	40	0.04	391	7162
ZnO/RhB	133	0.157	0.091	0.010	33	0.01	490	1490
ZnO/AO	218	0.165	0.102	0.014	39	0.02	524	2410
ZnO/C	357	0.476	0.320	0.073	43	0.07	295	2618
TZO/EY	379	1.027	0.803	0.213	55	0.21	85	3532
TZO/FGF	239	0.256	0.160	0.024	39	0.02	363	2540
TZO/Rose	298	0.688	0.459	0.089	44	0.09	139	1579
TZO/RhB	143	0.205	0.104	0.008	28	0.01	438	721
TZO/AO	283	0.177	0.106	0.019	39	0.02	484	2632
TZO/C	261	0.264	0.160	0.026	38	0.03	405	2003

the electrolyte must be suppressed under dark or illuminated conditions. Under normal DSSC operation, photo-generated carriers ideally collect at the FTO, but carrier loss can occur when they are injected into the electrolyte and collect at the platinum-coated FTO. As discussed in Ref. 28, surface states of metal oxide material have played a large role in the charge transport process. So, we believe that the injection of carriers from the conduction band of metal oxide into the electrolyte happens through surface states at the metal oxide/dye/electrolyte interface. Due to the large surface area of the device and also very small photo-absorption in oxide film, carrier loss due to recombination in the bulk of oxide is much less than that of the carrier loss through the interface. Recombination at the interface mainly occurs through surface defects in two ways. Firstly, this is by the transition of an electron from the conduction band of oxide to the highest occupied molecular orbitals (HOMO) state of an oxidized dye molecule through diffusion and surface states, as discussed in our earlier report.[28] Secondly, an electron is trapped at oxide surface states, which then react with I_3^- ions and form I^- ions (reduction process in the electrolyte). Recombination of electrons at the oxide/electrolyte occurs through surface states. In both cases, carrier loss is due to surface states.

Series resistance is less in the case of TZO as is clear from Table II. From a lower charge transfer resistance, a large electron injection driving force and, as a consequence, a larger J_{sc} can be obtained. The *J–V* performance of the dye-sensitized TZO electrode shows a decrease in the recombination rate, with a large increase in device power conversion efficiency. The dark current of TZO film is less than TiO_2 and ZnO, when compared in dark *J–V* graphs (Figs. 3, 4, 5). The higher dark current in the ZnO cells is indicative of faster electron recombination with the electrolyte than the bilayer structure.[42] The observed decrease in dark current is essentially due to the suppression of I_3^- reduction at the dye-sensitized TZO electrode/electrolyte interface. Also, it is reported in the literature that bilayer films have higher IPCE values due to better charge separation by a fast electron transfer process using two semiconductors with different conduction band edges and energy positions. The use of nanocrystalline TiO_2 permits the formation of an energy barrier at the ZnO electrode/electrolyte interface due to the fact that TiO_2 conduction band edge is more negative than ZnO. This energy barrier reduces the back electron transfer from the conduction band of ZnO to I_3^- in the electrolyte, thus reducing the recombination rate and improving the cell performance. Also, from XRD analysis,[22] we found that TZO has a large crystallization as compared to ZnO and TiO_2, which is in favor of reducing the energy losses of electron travelling in the semiconductor photoelectrodes film. TZO film has broader UV absorption range.[22] From photoconductivity measurements, we found that TZO has higher photosensitivity as compared to TiO_2 and ZnO.[22] So, another explanation is that, due to the TiO_2 layer on ZnO, ZnO forms a compact layer between FTO/TiO_2 which benefits the fast electron transfer from TiO_2 to ZnO to FTO glass and reduces the charge recombination occurring at the ZnO/FTO interface. ZnO cells have higher efficiency than TiO_2-based cells. In general, xanthene dyes such as Rose or EY have a better performance when used to sensitize ZnO rather than TiO_2 cells.[43] From *I–V* measurements, it has been found that EY dye is the most photosensitive dye for TZO and ZnO-based solar cells. Rose dye is the next most photosensitive dye that provides good photocurrent value. C dye is

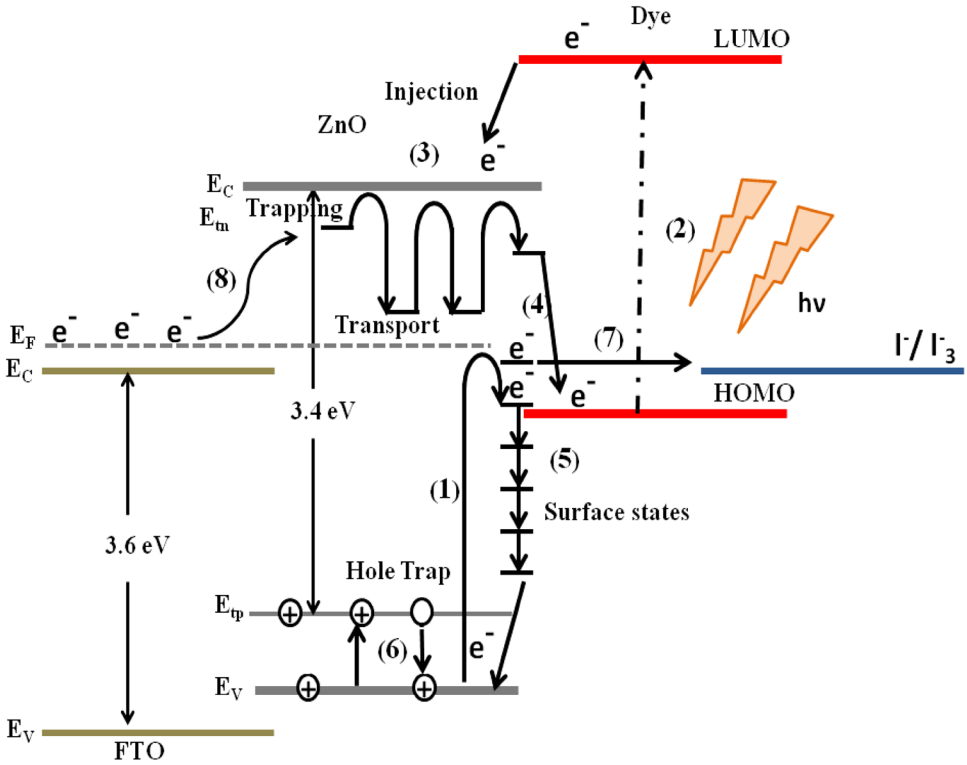

Fig. 12. Schematic representation of energy levels of FTO/ZnO/dye/electrolyte for significant (*1*) photo excitation of electrons into surface states, (*2*) photo excitation of electrons from HOMO to LUMO (lowest unoccupied molecular orbital) of the dyes, (*3*) injection from LUMO of dyes to ZnO CB ,(*4*) transport of electrons through electron traps to HOMO of dyes, (*5*) subsequent electron transfer between distributed surface states and recombination with holes in the valence band, (*6*) hole capture and thermal detrapping processes, (*7*) injection carrier from surface states of metal oxide to the electrolyte, and (*8*) electron injection from FTO to trap states of ZnO.

more photosensitivite for ZnO-based solar cells, but photocurrent decreases for TZO-based cells. The photocurrent of AO-sensitized ZnO is insufficient due to insufficient bonding between ZnO and AO, because of the absence of any anchoring group,[44] although the efficiency of cells is not high as these photoelectrodes were prepared 2 months before their characterization. It is well known that most of the organic dyes undergo degradation when they are adsorbed on the surface of a semiconductor, such as TiO_2 or ZnO, which can cause catalytic photodegradation. In addition, reactive oxygen species (mainly oxygen ions) may be formed with time, which react with oxidized dye molecules under visible or ultraviolet light irradiation in the presence of TiO_2 particles.[45,46] As a result of this reaction, the number of oxidized dye molecules may reduce. Dye degradation also depends on the adsorption sites[47] and constitutes a major problem, not only for the simple organic dyes but also for the highly efficient metal complex dyes.[48]

The V_{oc} is related to the interfacial charge recombination process between the dye-sensitized heterojunction and electrolyte. In open circuit conditions, all photo-generated carriers recombine within the solar cell diode.[49] Thus, if recombination can be minimized, V_{oc} can approach more closely to the maximum values. Also, we used potassium iodide (KI), but the solubility of KI in organic ethylene carbonate (EC) was quite low. So, a higher concentration of KI in EC could not be achieved. Due to the low solubility of the KI, there are fewer iodide ions in the electrolyte resulting in a low concentration of tri-iodide in the cell and, consequently, in the production of a relatively low current. So, an interesting step forward from this developed work, to improve the solar cell efficiency, will be to replace KI with organic tetrapropylammonium iodide (TPAI) and to incorporate Ag and Au nanoparticles in highly efficient TZO film, which will definitely improve the value of J_{sc} and V_{oc}.

CONCLUSIONS

In summary, the photoelectrochemical performance of porous ZnO, TiO_2 and bilayer TiO_2/ZnO (TZO) solar cells have been investigated by employing five organic dyes, plus a cocktail dye composed of the five dyes, as sensitizers. UV–Vis absorption spectra of all dye-sensitized oxide films confirms the anchoring of the dyes with all the ZnO, TiO_2 and TZO films. The device mechanism is controlled by thermionic emission at lower voltages, followed by space charge-limited current at higher voltages. It was observed that TZO films have a higher efficiency with the five organic dyes than

ZnO and TiO_2 solar cells, which is due to improved values of V_{oc} and J_{sc}. This may be due to the formation of energy barriers at the ZnO electrode/electrolyte interface because of the presence of the TiO_2 layer. This reduces the back electron transfer from CB of ZnO to I_3^- in the electrolyte, thus reducing the recombination rate and improving the cell performance. Also, TZO film has high crystallinity, broad UV absorption and higher photosensitivity as compared to ZnO film. ZnO forms a compact layer between FTO/TiO_2 which benefits the fast electron transfer from TiO_2 to ZnO to FTO glass and reduces the charge recombination occurring at the ZnO/FTO interface. Eosin-Y dye gave the best performance as a sensitizer with both ZnO and TZO. The lowest efficiency of TiO_2-based cells was with Xanthene dye which gives the best results with ZnO and photocatalytic degradation of dye by TiO_2.

ACKNOWLEDGEMENT

This work is financially supported by University Grant Commission (U.G.C.) New Delhi (Major Research Project). Mamta Rani would like to acknowledge the Council of Scientific and Industrial Research (CSIR), New Delhi, for providing fellowship. The authors are grateful to Hemant Singh, Indraprastha University, New Delhi, for sharing his research experience, fruitful discussions and support for solar cell measurements. The authors are also grateful to Solar Energy Centre, MNRE, Government of India, for providing the facility for photovoltaic measurements.

REFERENCES

1. B.O. Regan and M. Grätzel, *Nature* 35, 737 (1991).
2. A. Hagfeldt, G. Boschloo, L. Sun, L. Kloo, and H. Pettersson, *Chem. Rev.* 110, 6595 (2010).
3. R. Jose, V. Thavasi, and S. Ramakrishna, *J. Am. Ceram. Soc.* 92, 289 (2009).
4. B.P. Fingerhut, W. Zinth, and R.D. Vivie-Riedle, *Phys. Chem. Chem. Phys.* 12, 422 (2010).
5. P. Cheng, C.S. Deng, D.N. Liu, and X.M. Dai, *Appl. Surf. Sci.* 254, 3391 (2008).
6. S.S. Kim, J.H. Yum, and Y.E. Sung, *Sol. Energy Mater. Sol. C* 79, 495 (2003).
7. S. Kushwaha and L. Bahadur, *Int. J. Hydrog. Energy* 36, 11620 (2011).
8. J.Y. Liao and K.C. Ho, *Sol. Energy Mater. Sol. C* 86, 229 (2005).
9. A. Kitiyanan and S. Yoshikawa, *Mater. Lett.* 59, 4038 (2005).
10. A. Fukui, R. Komiya, R. Yamanaka, A. Islam, and L. Han, *Sol. Energy Mater. Sol. C* 90, 649 (2006).
11. H.K. Singh, S. Aggarwal, D.C. Agrawal, P. Kulria, S.K. Tripathi, and D.K. Avasthi, *Vacuum* 87, 21 (2013).
12. G.C. Vougioukalakis, A.I. Philippoulos, T. Stergiopoulos, and P. Falaras, *Coord. Chem. Rev.* 255, 2602 (2011).
13. S.A. Haque, Y. Tachibana, R.L. Willis, J.E. Moser, M. Grätzel, D.R. Klug, and J.R. Durrant, *J. Phys. Chem. B* 104, 538 (2000).
14. J. Nelson, S.A. Haque, D.R. Klug, and J.R. Durrant, *Phys. Rev. B.* 63, 205321 (2001).
15. M. Grätzel, *J. Photochem. Photobiol. C* 4, 145 (2003).
16. S.J. Kang, *J. Korean Phys. Soc.* 47, 589 (2005).
17. H. Guo, J. Zhou, and Z. Lin, *Electrochem. Commun.* 10, 146 (2008).
18. W. Wu, S. Bai, N. Cui, F. Ma, Z. Wei, Y. Qin, and E. Xie, *Sci. Adv. Mater.* 2, 402 (2010).
19. A. Umar, M.S. Akhtar, S.H. Kim, A. Al-Hajry, M.S. Chauhan, and S. Chauhan, *Sci. Adv. Mater.* 3, 695 (2011).
20. T.P. Chou, Q.F. Zhang, and G. Cao, *J. Phys. Chem. C* 111, 18804 (2007).
21. Y. Xu and M.A.A. Schoonen, *Am. Mineral.* 85, 543 (2000).
22. M. Rani and S.K. Tripathi, *Energy Environ. Focus* 2, 227 (2013).
23. S.S. Mali, C.A. Betty, P.N. Bhosale, and P.S. Patil, *Electrochim. Acta* 59, 113 (2012).
24. Z.F. Fang, L.X. Ping, Z.J. Bo, Z.X. Wen, and L. Yuan, *Chin. Sci. Bull.* 54, 2633 (2009).
25. N. Khongchareon, S. Choopuna, N. Hongsith, A. Gardchareon, S. Phadungdhitidhada, and D. Wongratanaphisan, *Electrochim. Acta* 106, 195 (2013).
26. K. Hongsith, N. Hongsith, D. Wongratanaphisan, A. Gardchareon, S. Phadungdhitidhada, P. Singjai, and S. Choopun, *Thin Solid Films* 539, 260 (2013).
27. P.K. Baviskar, J.B. Zhang, V. Gupta, S. Chand, and B.R. Sankapal, *J. Alloy Compd.* 510, 33 (2012).
28. M. Rani and S.K. Tripathi, *Mater. Sci. Eng. B* 187, 214 (2014).
29. M. Rani and S.K. Tripathi, *J. Electron. Mater.* 43, 426 (2014).
30. S. Rani, P.K. Shishodia, and R.M. Mehra, *J. Renew. Sustain. Energy* 2, 0431031 (2010).
31. K. Hara, Z.S. Wang, T. Sato, A. Furube, R. Katoh, H. Sugihara, Y. Dan-oh, C. Kasada, A. Shinpo, and S. Suga, *J. Phys. Chem. B* 109, 15476 (2005).
32. J.J. Liou and J.S. Yuan, *Semiconductor Device Physics and Simulations* (New York: Plenum Press, 1998), p. 8.
33. S.M. Sze, *Physics of Semiconductor Devices*, 1st ed. (New York: Wiley, 1981), p. 146.
34. S. Monticone, R. Tufeu, A.V. Kanaev, E. Scolan, and C. Sanchez, *Appl. Surf. Sci.* 162, 565 (2000).
35. J. Pascual, J. Camassel, and H. Mathieu, *Phys. Rev. Lett.* 39, 1490 (1977).
36. M.D. Stamate, *Appl. Surf. Sci.* 205, 353 (2003).
37. M.K. Nazeeruddin, F. De Angelis, S. Fantacci, A. Selloni, G. Viscardi, P. Liska, S. Ito, B. Takeru, and M. Grätzel, *J. Am. Chem. Soc.* 127, 16835 (2005).
38. S. Aydogan, M. Saglam, and A. Türüt, *Appl. Surf. Sci.* 250, 43 (2005).
39. M. Pattabi, S. Krishna, N. Ganesh, and X. Mathew, *Sol. Energy Mater. Sol. Cells* 81, 111 (2007).
40. T.G. Abdel Malik and R.M. Abdel-Latif, *Thin Solid Films* 305, 336 (1997).
41. H.M. Zeyada, M.M. El-Nahass, and E.M. El-Menyyawy, *Sol. Energy Mater. Sol. C* 92, 1586 (2008).
42. M.K.I. Senevirathne, P.K.D.D.P. Pitigala, V. Sivakumar, P.V.V. Jayaweera, A.G.U. Perera, and K. Tennakone, *J. Photochem. Photobiol. A* 195, 364 (2008).
43. E. Guillén, F. Casanueva, J.A. Anta, A. Vega-Poot, G. Oskam, R. Alcántara, C. Fernández-Lorenzo, and J. Martín-Calleja, *J. Photochem. Photobiology A* 200, 364 (2008).
44. F. Labat, I. Ciofini, H.P. Hratchian, M.J. Frisch, K. Raghavachari, and C. Adamo, *J. Am. Chem. Soc.* 131, 14290 (2009).
45. F. Zhang, J. Zhao, L. Zang, T. Shen, H. Hidaka, E. Pelizzetti, and N. Serpone, *J. Mol. Catal. A* 120, 173 (1997).
46. T. Wu, G. Liu, J. Zhao, H. Hidaka, and N. Serpone, *J. Phys. Chem. B* 102, 5845 (1998).
47. H. Tributsch, *Coord. Chem. Rev.* 248, 1511 (2004).
48. B. Macht, M. Turrion, A. Barkschat, P. Salvador, K. Ellmer, and H. Tributsch, *Sol. Energy Mater. Sol. C* 73, 163 (2002).
49. G. Boschloo and A. Hagfeldt, *Acc. Chem. Res.* 42, 1819 (2009).